Journal of Molecular Graphics and Modelling 28 (2009) 156–161

Contents lists available at ScienceDirect

Journal of Molecular Graphics and Modelling

journal homepage: www.elsevier.com/locate/JMGM

Superoxide interaction with nickel and iron superoxide dismutases

Radu Silaghi-Dumitrescu *

Department of Chemistry, "Babes-Bolyai" University, Cluj-Napoca RO-400028, Romania

ARTICLE INFO

Article history:
Received 24 October 2008
Received in revised form 9 June 2009
Accepted 10 June 2009
Available online 18 June 2009

Keywords:
Superoxide dismutase
Nickel
Non-heme iron
Superoxide
Density functional theory
Superoxide reductase

ABSTRACT

Interaction of superoxide with the metal active sites of nickel and iron-containing superoxide dismutases is investigated with density functional theory. Outer-sphere mechanisms for both the reduction and oxidation of superoxide are proposed to be the common feature of these structurally unrelated SODs.

1. Introduction

Superoxide is a key component of oxidative stress *in vivo*, and its removal by specialized metalloenzymes, superoxide dismutases (SODs) and superoxide reductases (SORs), is essential for living organisms [1]. The mechanisms of enzymatic superoxide reduction have been studied extensively but remain incompletely understood. Three main classes of SODs are known. The Fe/MnSODs feature a five-coordinate Fe or Mn center, and are structurally (and presumably, mechanistically) extremely similar to each other. A second, more recently discovered, class of SODs contains Ni at their active sites [1]. Proposed catalytic mechanisms for the Fe- and NiSODs are shown in Fig. 1. While no metal-superoxide adducts have been demonstrated as catalytic intermediates for any SOD so far, such adducts have often been proposed [2]. For Ni-SOD, a proposed catalytic cycle (cf. Fig. 1) [2] involves superoxide binding to Ni(II), to form a Ni(II)-superoxo adduct, which undergoes a proton-dependent decay to Ni(III) and H_2O_2. Subsequent binding of superoxide to the Ni(III) center leads to a Ni(III)-superoxo adduct, which decays to Ni(II), liberating dioxygen. Initial structural data on NiSOD indicated the Ni coordination in the resting state to be square planar, as shown in Fig. 1 [3]; however, more recent crystallographic work indicates additional ligation of a histidine side-chain to the Ni(III) state (cf. Scheme 1) [2]. Although particularly weak (the minimum Ni-His distance found by crystallography is 2.6 Å, 0.5 Å longer than typical Ni–nitrogen bond lengths) [2], this latter interaction occurs trans to the putative superoxide binding position and has therefore been proposed to promote dioxygen release; axial His ligation/deligation may in principle also help bring the Ni(III/II) redox potential into the range required for outer-sphere superoxide dismutation. The third known class of SODs contain a zinc–copper binuclear active site; here again outer-sphere and inner-sphere mechanisms have been proposed, with the latter recently shown to be feasible computationally [1,4–6].

Here, density functional calculations are reported on the interaction of superoxide with the mononuclear active sites of nickel and iron-containing SODs, aimed to identify possible underlying common features of enzymatic superoxide dismutation. Siegbahn and co-workers have also reported a computational study on NiSOD [7]. An inner-sphere mechanism possibly requiring protonation of a cysteine ligand was proposed [7]; although our results also support the possibility of superoxide-metal ligands (possibly driven by protonation), we find that Ni-SOD activity can be rationalized without invoking such adducts, and that indeed catalytically competent superoxide oxidation/reduction may be achieved by the nickel center without proper formation of a nickel–oxygen bond. These conclusions appear to place the FeSOD mechanism in a new light.

2. Methods

Fig. 1 illustrates the structures of the basic models used in the present work. We note that with a pK_a of 4,9, superoxide (OOH^0), is

* Tel.: +40 264593833; fax: +40 264590818.
E-mail address: rsilaghi@chem.ubbcluj.ro.

1093-3263/$ – see front matter © 2009 Elsevier Inc. All rights reserved.
doi:10.1016/j.jmgm.2009.06.001

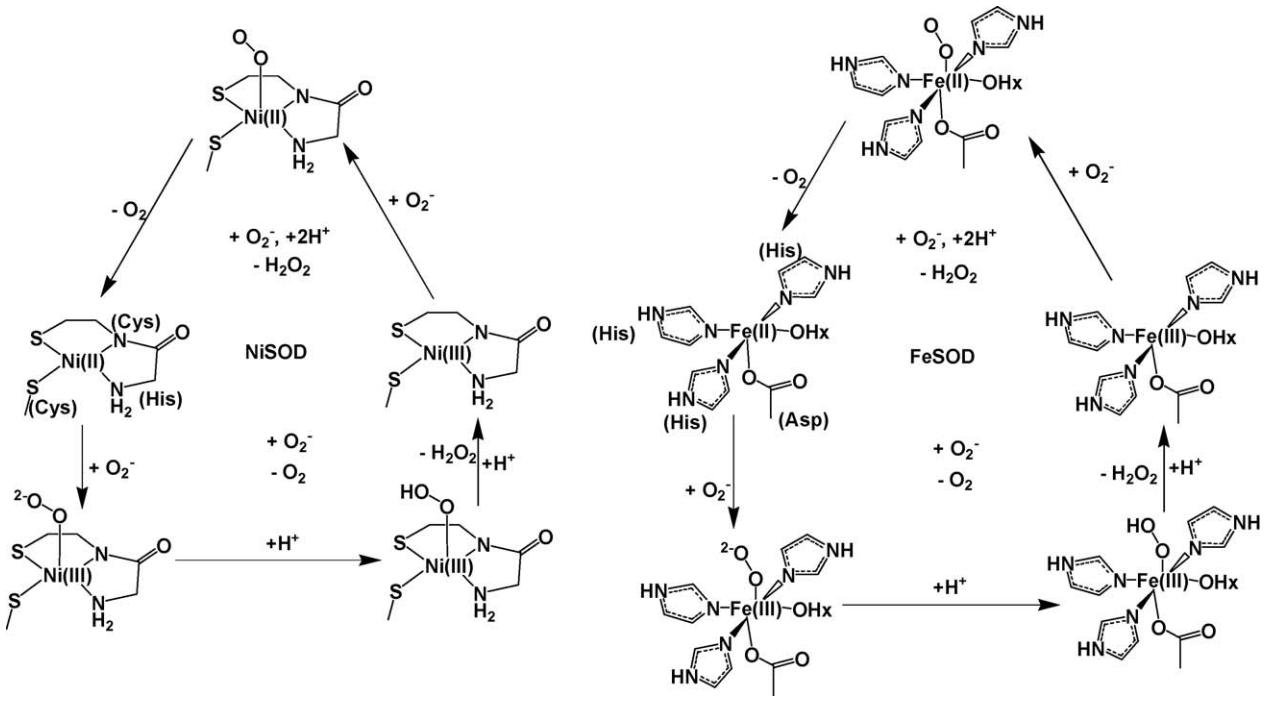

Fig. 1. Proposed catalytic cycles for NiSOD and FeSOD. Straight arrows indicate inner-sphere mechanisms, including putative metal-superoxide adducts. Curved arrows indicate outer-sphere mechanisms. The active sites are drawn as employed in the models used in the present study. The identity of protein residues providing metal ligands is indicated in parentheses.

essentially entirely deprotonated at physiological pH (O_2^-), and therefore the models examined here are the products of putative reactions between metal centers and O_2^-, rather than OOH^0 (though subsequent protonation of the metal–OO species is still investigated). The starting coordinates for NiSOD models were taken from the crystal structure of the active NiSOD (pdb code 1T6U) [3]. Geometries for NiSOD models were optimized without any constraints. The starting coordinates for FeSOD models were taken from the crystal structure of resting FeSOD (pdb code 1BSM [8]). Geometries for FeSOD models were optimized by freezing the coordinates of the heavy atoms within the protein-derived iron ligands, in order to avoid massive rearrangement of the imidazole and carboxylate ligands to relative orientations that would impose steric and electronic constraints not present and thus not directly relevant to the FeSOD active site; such rearrangement does not occur in the NiSOD models. This approach for treating enzyme active sites has been verified with a number of related models; it has the advantage of allowing a relaxation of the iron coordination sphere (as the iron and the water/hydroxo and superoxo ligands are free to move) to accommodate changes in charge and spin state, while also preserving geometrical features of the active site which are clearly imposed by the larger protein/solvent environment [9–11]. An alternative to this approach [4,11] would be to include in the model atoms found further away from the metal, such as the apha carbons of aminoacids coordinated to the metal, freeze the coordinates of these distant atoms during the geometry optimization procedure, and allow the rest of the coordination sphere to optimize freely. As pointed out before, this approach does not conserve key geometrical features of the active site, such as dihedral angles between imidazole and carboxylate planes, and their relative orientations towards the metal [10–12]. Unless otherwise specified, imidazole rings are assumed monoprotonated (neutral), while carboxylates and cysteinates are assumed anionic (deprotonated). Metal and peroxo/superoxo oxidation states of each model are listed in figure legends and table.

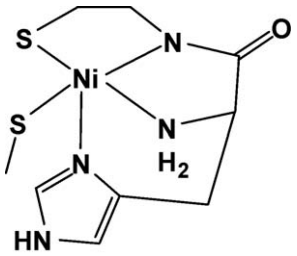

Scheme 1.

The UBP86 functional, which uses the gradient-corrected exchange functional proposed by Becke [13], the correlation functional by Perdew [14], and the DN** numerical basis set (comparable in size to 6-31G**) were used as implemented in Spartan [15]. For the SCF calculations, a fine grid was used, and the convergence criteria were set to 10^{-6} (for the root-mean square of electron density) and 10^{-8} (energy), respectively. For geometry optimization, convergence criteria were set to 0.001 au (maximum gradient criterion) and 0.0003 (maximum displacement criterion). Net charges and spin states on the models are shown. Partial atomic charges and spin densities were derived from Mulliken population analyses after DFT geometry optimization. Activation energies were not explicitly calculated, as most of the processes for which these would be sought have already been calculated by Siegbahn and co-workers, who found them to be very low and hence the processes would be quite facile [7]. The results do come with a caveat, in that the active sites models employed here include only the first coordination sphere of the metal in a gas-phase, and do not account directly for the larger protein and solvent environment. Nevertheless, our previous experience with models of similar chemistry, charge and/or size suggest that geometries obtained at this level can be reliable, and that trends in energy differences will be conserved after applying solvent corrections [9–11,16–20].

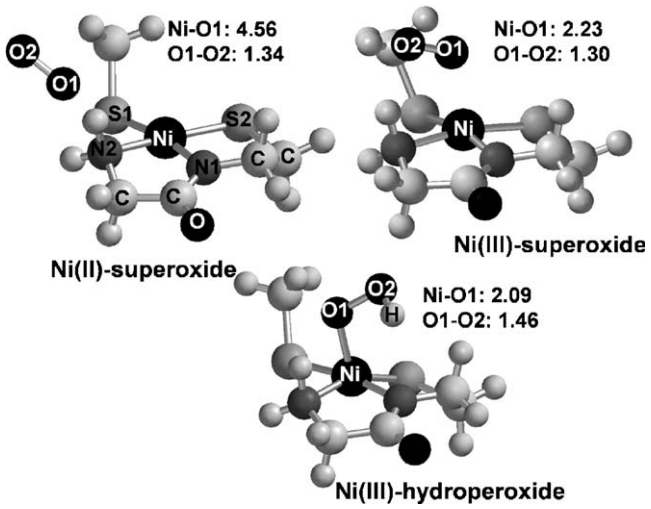

Fig. 2. Optimized geometries for NiSOD models.

3. Results and discussion

Fig. 2 shows optimized geometries for models of putative Ni(II)-superoxo and Ni(III)-superoxo NiSOD adducts proposed to form within the NiSOD catalytic cycle. Contrary to expectations based on Fig. 1, superoxide moves away from the nickel center simply upon geometry optimization of the S = 1/2 "Ni(II)-superoxide" model. The superoxide moiety instead prefers to hydrogen bond to amine protons in the model, retaining an O–O bond length (1.34 Å) and spin density (1.04) consistent with a free superoxide moiety rather than peroxide. These findings argue against a Ni(II)-superoxide bond being formed within the NiSOD catalytic cycle, and suggest that reduction of superoxide to peroxide by Ni(II)-SOD must instead be proton-driven. A small model compound containing an S = 1/2 Ni(II)-superoxo adduct has recently been described experimentally and computationally, with four neutral equatorial nitrogen ligands and an axial superoxide ligand featuring one Ni–O bond at ~2 Å [21]. By comparison, our results now illustrate the extent to which the three anionic and strongly interacting equatorial ligands in NiSOD can disfavour binding of superoxide (and presumably other exogenous ligands) to the metal center.

An S = 1/2 Ni(III)–OOH model, formally the product of protonated superoxide binding to Ni(II), featured a 1.47-Å O–O bond and only 0.34 unpaired spins located on the oxygen atoms as opposed to 0.50 spins located on nickel—consistent with a Ni(III)-hydroperoxide description. The Ni(III)–OOH model was then re-optimized constraining the Ni–OOH distance to 3 Å, where negligible Ni–O bonding is expected compared to the equilibrium structure. Even in this model, the O–O distance remained consistent with peroxide (1.41 Å), and only ~0.3 spin units were localized on the OOH moiety. This result suggests that an incoming protonated superoxide moiety (HO_2) would be immediately reduced in an outer-sphere manner, without any *need* for "proper" Ni–O bond formation. Ni–O bond formation is thus not a prerequisite for, although it still may be a *consequence* of superoxide reduction by NiSOD. This deduction is in fact consistent with the outer-sphere azide modelled into Ni(III)-SOD active site in Ref.[3], although not with the superoxide modelled into the Ni(II) site. On the other hand the proximal hydrogen bonded Tyr5 or nearby waters could donate a proton prior to or concerted with outer-sphere superoxide reduction. Siegbahn and co-workers, in their recent computational study [7], have found that the barrier for Ni(III)–OOH bond formation (species 4 going to species 5 in their Fig. 5) is essentially inexistent, and that this binding involves essentially no change in the energy of the system; thus, an OOH^- moiety subjected to outer-sphere electron transfer does have two equally feasible options available—escape into solution (where protonation would be immediate and essentially barrierless given the peroxide pK_a of ~11.7) or bind to the metal. If a metal–OOH bond IS formed, then it follows from Siegbahn et al.'s results that its decay prior to protonation (species 5 reverting to species 4 in their Fig. 5 [7]), to liberate OOH^- which would then undergo facile protonation, is essentially barrierles; alternatively, Siegbahn and co-workers also find that protonation of the metal-bound OOH– to produce HOOH would be extremely facile, involving a barrier of 11.5 kcal/mol [7]; since their proposed proton donor is a protonated cysteine ligand of the nickel, and since no experimental evidence is to our knowledge available to support such protonation (unlike the well-documented deprotonation of iron-bound water in FeSODs), it appears that both our results and those from Siegbahn and co-workers converge towards a mechanism where metal-peroxide bond formation is possible but is *not as a prerequisite for OOH^- protonation and reduction*.

For the S = 1 Ni(III)-superoxide adduct, a 2.23-Å Ni–OO bond is predicted which is distinctly longer than typical metal-superoxo or metal-peroxo bonds [12,17,18,22,23], and 1.42 unpaired electrons are found to reside on the dioxygenic ligand [24]. This points towards a Ni(II)-dioxygen description. The O_2 moiety is expected to be liberated extremely easily due to the solvent exposure of the active site (cf. Fig. 3); dioxygen binding to metalloproteins is generally controlled by the hydrophobicity of the dioxygen binding site [25]. Indeed, replacing the dioxygen ligand in the Ni(II)-SOD-dioxygen model with a single water molecule was found to cost only ~1 kcal/mol [26]. With the NiSOD active site relatively exposed to solvent (see below), the local concentration of water will be several orders of magnitude higher than that of dioxygen, thereby generating a strong driving force for displacement of dioxygen away from the active site. The nickel–oxygen distance computed in this model is likely an underestimate due to the small size of the gas-phase model employed. A local minimum was additionally identified for the Ni(III)-superoxide model, with a Ni–O distance of 2.96 Å. This structure was very similar to that shown in Fig. 2, in that it featured an O–O bond of 1.28 Å and 1.37 spin units on the dioxygenic ligand. Thus, even at an essentially non-bonding Ni–OO distance of 3 Å, the system is reasonably well described as Ni(II) + dioxygen, implying that superoxide needs not form a proper Ni–O bond in order to transfer its electron. This, together with the significant solvent accessibility of the Ni site, argues for an entirely outer-sphere mechanism of superoxide oxidation by NiSOD.

Initial structural data on NiSOD indicated the Ni coordination to be square planar [3]; however, more recent crystallographic work indicates additional very weak ligation of a histidine side-chain to the Ni(III) state [2]. To investigate the importance of this histidine, two more classes of models were used, derived from those in Fig. 2. First, an ammonia moiety (mimicking the imidazole side-chain) was placed trans to the O_2; this addition did not affect the equilibrium geometry and electronic structure of the Ni(II)-dioxygen moiety to any significant extent (data not shown). However, placing an ammonia moiety trans to the OOH ligand in the Ni(III)-hydroperoxo model resulted in elongation of the Ni–OOH bond by 0.15 Å; additionally, an ammonia–nickel–oxygen angle of 165° was found in this geometry, further illustrative of a weak Ni–OOH interaction in this ammonia model. A role for the histidine ligand in obstructing hydroperoxide binding to the site may then be proposed. A second class of improved models included the His side-chain explicitly, cf. Scheme 1, at starting Ni–N distances of 2.2–2.6 Å. In this series of models, the Ni–O–O moiety in the Ni(III)-superoxo adduct appeared essentially identical to its counterpart in Fig. 2 (S = 1 state 21 kcal/mol below the S = 0 state), with the imidazole moiety de-ligated from the metal upon

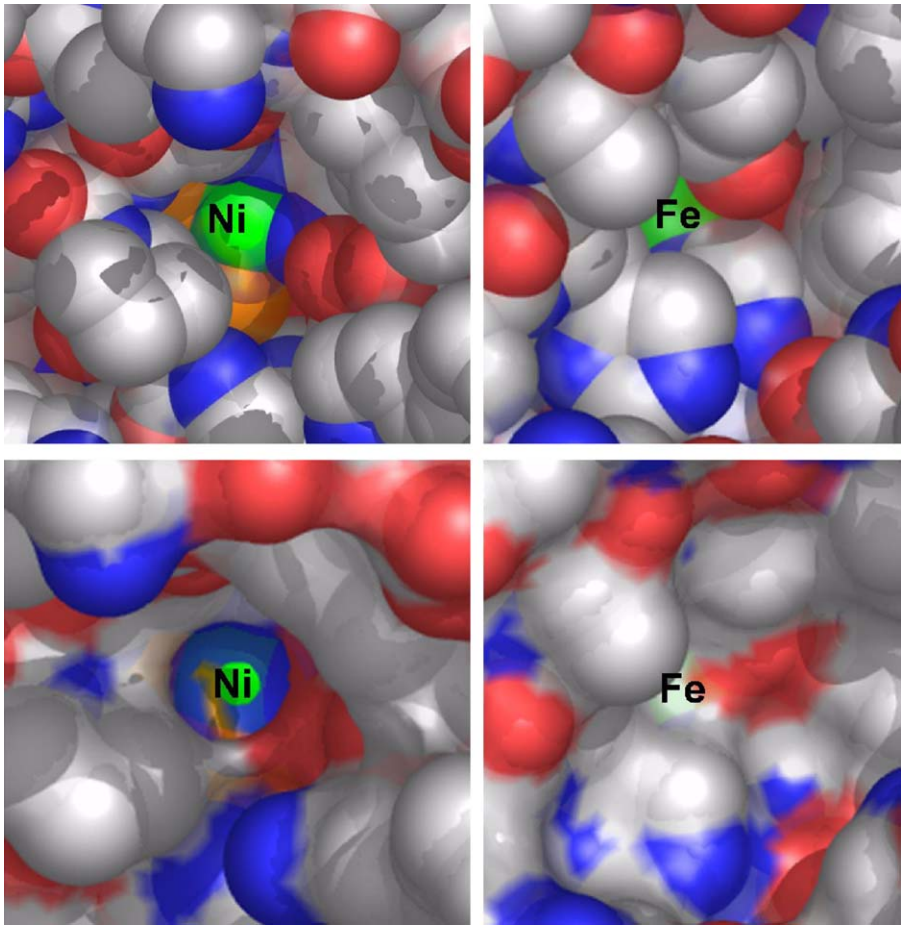

Fig. 3. Spacefill representations of the crystal structures of Ni-SOD (pdb code 1T6U) and Fe-SOD (pdb code 1BSM), illustrating different degrees of accessibility of the metal sites. Superimposed over the crystal structures are solvent accessibility surfaces calculated with a 1.6-Å probe. For each protein, the top and bottom views differ by the extent of transparency of the calculated surface. The top views illustrate how the Ni and Fe sites are both reasonably close to the surface; while access to Ni appears relatively straightforward, the Fe atom is barely visible in the top view, and the bottom view shows how access to Fe is in fact completely obstructed by surface amino acid residues. Color coding: carbon: grey; nitrogen: blue; oxygen: red; sulphur: yellow; metal: green. Figure rendered in Pymol [51].

geometry optimization. Likewise, the imidazole–Ni bond was broken upon geometry optimization of the Ni(III)-hydroperoxo model, which otherwise appeared essentially identical to its counterpart in Fig. 2. Finally, for the imidazole-Ni(II)-superoxide model, geometry optimization resulted in de-ligation of two ligands (NH_2 and the thiolate trans to it, cf. Scheme 1); if these two latter bond lengths were frozen, then the imidazole ligand dissociated, returning the model to the same state as its counterpart in Fig. 2. In conclusion, it appears that if the protein can enforce axial ligation by His a histidine at its active site, the effect is labilization of the other Ni-ligand bonds; this may be important in avoiding inhibitor binding (where the inhibitor may be the product, peroxide, or any other small molecule present *in vivo*). Wuerges et al. have found that indeed the Ni-'axial' histidine distance varies in Ni-SOD crystal structures, where it is seen as short as 2.6 Å; they further demonstrated that further elongation ensued upon exposure of the crystal to X-rays, implying that, in principle, the iron–histidine may in reality be even shorter than 2.6 Å.

Brunold and co-workers reported an extensive spectroscopic and computational study of NiSOD resting states [27]. They pointed out that azide, a typical anionic ligand for metalloproteins, does not bind to the Ni center, although a binding site *near* the metal is suggested by MCD and EPR data [27] and is consistent with the presence of positively charged residues proposed to guide superoxide anions towards the active site, in what appears to be a common theme of superoxide-reacting enzymes [3,28]. This lack of coordination is consistent with the above-reported refusal of superoxide to bind to Ni(II)SOD, and is consistent with the d^8 configuration of the metal with no empty orbitals available for interaction with incoming anionic ligands such as azide or superoxide—in contrast to the better-characterized interaction of superoxide with d^6 Fe(II) [12]. Based on the lack of azide coordination, Brunold and co-workers hypothesized that NiSOD would follow outer-sphere mechanisms. Our results now confirm their hypothesis [27].

In FeSOD, several possible spin states are in principle possible for the Fe(III) and Fe(II)-superoxo species. Table 1 shows that the most favoured spin state for Fe(III)-superoxide SOD is S = 3, where the Fe–OO distance is very long (~2.6 Å), and the OO moiety is reasonably well described as neutral dioxygen, i.e., electron transfer from superoxide to iron has already occurred, without any need to form an iron-superoxide bond. Other spin states are close in energy to S = 3; however, these energy differences are likely to be underestimated here, given the previously noted propensity of non-hybrid functionals to favour lower spin states [29–31].

The identity of the solvent ligand in FeSOD (OHx in Fig. 1) has been a matter of debate: although the iron–oxygen distance in SOD crystal structures is distinctly longer than expected for an Fe–OH interaction, evidence has been presented that in solution the solvent ligand may cycle between hydroxo and aqua, depending on the iron oxidation state [8,21]. Table 1 also lists data for the Fe(III)SOD-superoxide models assuming a hydroxo rather than

Table 1
Relative energies (kcal/mol), key bond lengths (Å) and cumulated spin densities on the dioxygenic ligand for FeSOD superoxide adducts. For Fe(III)–O_2^- models, values for models containing a hydroxo ligand instead of water (OHx in Fig. 1) are shown in italics, with S = 3 states are taken as references for relative energies. For Fe(II)–O_2^- models, the S = 1/2 state is taken as reference for relative energies.

	ΔE	Fe–O	O–O	OO spin
S = 0 Fe(III)-O_2^-	11	1.78	1.29	0.00
	−0.1	*1.79*	*1.30*	*0.00*
S = 1 Fe(III)-O_2^-	13.7	1.88	1.29	0.91
	−2.0	*1.87*	*1.31*	*0.70*
S = 2 Fe(III)-O_2^-	2.5	1.88	1.30	0.45
	−0.4	*1.97*	*1.31*	*0.09*
S = 3 Fe(III)-O_2^-	0.0	2.55	1.27	1.75
	0.0	*2.51*	*1.29*	*1.46*
S = 1/2 Fe(II)-O_2^-	0.0	1.86	1.36	0.58
S = 3/2 Fe(II)-O_2^-	6.1	1.88	1.37	0.02
S = 5/2 Fe(II)-O_2^-	1.2	1.94	1.38	0.99
S = 3/2 Fe(II)-O_2^- [a]	7.2	1.96/2.01[a]	1.41	0.22
S = 5/2 Fe(II)-O_2^- [a]	6.4	2.06/2.00[a]	1.43	0.82

[a] Bidentate binding of superoxide

aqua ligand. The hydroxo models are essentially degenerate in energy (with respect to each other). This implies that the S = 3 state, and implicitly the outer-sphere mechanism, is entirely accessible. In fact, given the above-mentioned caveat on non-hybrid functionals favouring lower spin states, we may expect that in reality the S = 3 state will be favoured over all others.

Thus, the Fe(III)SOD + superoxide interaction will most likely be outer-sphere, with charge transfer from superoxide to iron occurring prior to formation of a Fe–OO bond.

Cano and co-workers have examined the Fe(II)SOD + superoxide interaction elsewhere, showing that a S = 5/2 state is favoured and the system is best described as containing an Fe(III)-center bound to peroxide [32]. Our own data (cf. Table 1) is in general agreement with these findings. In all spin states and regardless of hapticity, the OO ligand features a bond length consistent with peroxide, although large amounts of spin do seem to be delocalized onto the oxygen atoms, as previously noted for other formally ferric-peroxo adducts [12]. The S = 5/2 state of a monodentate Fe(II)-O_2^- adduct is predicted here (cf. Table 1) to be only 1 kcal/mol above the S = 1/2 state, which, based on similar considerations as for Fe(III)-O_2^-, may be interpreted to mean that within a protein environment the S = 5/2 state would in fact be favoured. Perhaps not to be ignored is the existence of a S = 5/2 side-on isomer, only 5 kcal/mol above end-on S = 5/2. Given the error associated with the reduced size of the models used in this study, side-on binding of superoxide within the actual Fe(II)-SOD active site cannot be excluded. Side-on binding would in principle offer an advantage towards completion of the catalytic cycle with peroxide removal, in view of its distinctly elongated O–O bond length compared to other isomers suggestive of an increased peroxo character.

An SOD ferric-peroxo adduct, if ever formed, would have to decay via a ferric-hydroperoxo state. Table 2 illustrates relevant parameters for such a putative SOD Fe(III)–OOH adduct. The S = 1/2 and S = 5/2 states are essentially equal in energy, which, based on arguments similar to those exposed above for spin states of other adducts, implies that at the SOD active site the S = 5/2 state will be favoured. The Fe–OOH bond lengths are similar to those previously calculated for other iron complexes at the same level of theory: 1.82 Å for S = 1/2 SOD compared to 1.77–1.84 Å in other heme and non-heme models [12,17,18,33,34], 1.88 Å for S = 3/2 SOD compared to 1.84 Å in the corresponding superoxide reductase model, and 2.07 Å in S = 5/2 SOD compared to 1.99 and 2.03 in superoxide reductase and hemerythrin, respectively [12,34]. SOD ferric-hydroperoxo adducts are thus local minima even for the S = 5/2 state and with the solvent-derived ligand assumed to be hydroxide, i.e., under conditions where the Fe–OOH bond should be weakest. The O–O bond lengths and spin densities are all consistent with a ferric-hydropero electronic description, as opposed to a ferrous-superoxide electromer.

Table 2
Relative energies (ΔE, kcal/mol), key bond lengths (Å) and cumulated spin densities on the dioxygenic ligand for FeSOD ferric-hydroperoxo adducts. The S = 1/2 state is taken as reference for relative energies.

	ΔE	Fe–O	O–O	OOH spin
S = 1/2 Fe(III)–OOH	0	1.82	1.50	0.19
S = 3/2 Fe(III)–OOH	6.8	1.88	1.49	0.04
S = 5/2 Fe(III)–OOH	1	2.07	1.46	0.40

To summarize, the data shown here suggests that the interaction of superoxide with the oxidized metal active sites of NiSOD and FeSOD follows outer-sphere mechanisms. On the other hand, interaction of superoxide with the reduced SODs may well differ mechanistically: while an inner-sphere mechanism has previously been supported by computations and substrate analogue binding in FeSOD, we find that NiSOD is more likely to follow an outer-sphere mechanism.

If NiSOD, whose metal site is solvent-exposed, operates via an outer-sphere mechanism, it would be difficult to rationalize why FeSOD should operate via an inner-sphere mechanism, since its iron active site is buried with no well-defined access channel leading from surface to the metal (cf. Fig. 2). On the contrary, the solvent inaccessibility in FeSOD would be easier rationalized as being meant to prevent formation of a Fe(III)-peroxo species. Ferric-peroxo and ferric-hydroperoxo complexes can perform oxygenation reactions, and ferric-hydroperoxo complexes may additionally undergo O–O bond cleavage leading to strongly oxidizing high-valent iron species [16,18,35–40]; a possible notable exception to this rule is the solvent-exposed active site of superoxide reductase [41], where a ferric-peroxo intermediate is postulated. SOR's solvent exposure would allow facile superoxide binding and is also thought to be instrumental for peroxide release [12,42].

The NiSOD metal site needs not be protected by a protein barrier, as it intrinsically refuses to bind the superoxide anion; as proposed above, the presence of a histidine ligand trans to the putative superoxide binding site may have the additional role of preventing formation or destabilizing of a Ni-hydroperoxo adduct.

By contrast, reduction of superoxide by the ferrous center of superoxide reductase is currently believed to be at least partially driven by metal-superoxide coordination—with a role for protons also demonstrated [41].

If indeed FeSOD operates via an outer-sphere mechanism, then the presence of two coordination positions on the iron not occupied by the protein may be rationalized not as meant to allow binding of superoxide but simply as part of the strategy to dynamically adjust the redox potential of the center in order to efficiently alternate superoxide reduction with superoxide oxidation. The importance of tuning this redox potential via changes in ligation, including protonation/deprotonation steps, is discussed elsewhere [43]. Perhaps related to the outer-sphere hypothesis, in MnSOD, which is highly homologous to FeSOD but contains a manganese ion instead of iron, an inhibited state has been reported experimentally, which is described as a manganese-peroxide adduct whose relative stability is due to a damaged coordination environment around the metal (possibly a significantly elongated Mn-carboxylate bond compared to the resting state) [43]. The results reported herein on FeSOD suggest an alternative interpretation, where MnSOD would normally operate by an outer-sphere mechanism, and any manganese-peroxide adduct would

represent an inhibited state. A somewhat similar picture has been seen in superoxide reductases, where a ferric-peroxo adduct extensively characterized by spectroscopic [44–46] and computational [12,33,46] methods appears to be kinetically incompatible with turnover and thus represents an inhibited state; the existence of a kinetically competent ferric-peroxo adduct in SOR has however not been ruled out [47,48].

Alternatively, the available coordination positions on the iron in FeSODs may relate to an as yet unclear [49] additional mechanism/function of the enzyme (cf. "catalytic promiscuity" [50]).

Acknowledgements

Dr. I. Silaghi-Dumitrescu ("Babes-Bolyai" University, Cluj-Napoca) is thanked for helpful discussions and access to computational facilities. Dr. D.M. Kurtz, Jr. (University of Texas at San Antonio) is thanked for helpful discussions and critical comments to the manuscript.

References

[1] A.F. Miller, Superoxide dismutases: active sites that save, but a protein that kills, Curr. Opin. Chem. Biol. 8 (2004) 162–168.
[2] J. Wuerges, J.W. Lee, Y.I. Yim, H.S. Yim, S.O. Kang, K.D. Carugo, Crystal structure of nickel-containing superoxide dismutase reveals another type of active site, Proc. Natl. Acad. Sci. U.S.A. 101 (2004) 8569–8574.
[3] D.P. Barondeau, C.J. Kassmann, C.K. Bruns, J.A. Tainer, E.D. Getzoff, Nickel superoxide dismutase structure and mechanism, Biochemistry 43 (2004) 8038–8047.
[4] V. Pelmenschikov, P.E. Siegbahn, Copper–zinc superoxide dismutase: theoretical insights into the catalytic mechanism, Inorg. Chem. 44 (2005) 3311–3320.
[5] J.A. Tainer, E.D. Getzoff, J.S. Richardson, D.C. Richardson, Structure and mechanism of copper, zinc superoxide dismutase, Nature 306 (1983) 284–287.
[6] R. Konecny, J. Li, C.L. Fisher, V. Dillet, D. Bashford, L. Noodleman, CuZn superoxide dismutase geometry optimization, energetics, and redox potential calculations by density functional and electrostatic methods, Inorg. Chem. 38 (1999) 940–950.
[7] V. Pelmenschikov, P.E. Siegbahn, Nickel superoxide dismutase reaction mechanism studied by hybrid density functional methods, J. Am. Chem. Soc. 128 (2006) 7466–7475.
[8] M. Schmidt, Manipulating the coordination number of the ferric iron within the cambialistic superoxide dismutase of *Propionibacterium shermanii* by changing the pH-value A crystallographic analysis, Eur. J. Biochem. 262 (1999) 117–127.
[9] R. Silaghi-Dumitrescu, Nitrite linkage isomerism in cytochrome cd1 nitrite reductase, Inorg. Chem. 43 (2004) 3715–3718.
[10] R. Silaghi-Dumitrescu, Copper-containing nitrite reductase: a DFT study of nitrite and nitric oxide adducts, J. Inorg. Biochem. 100 (2006) 396–402.
[11] R. Silaghi-Dumitrescu, I. Silaghi-Dumitrescu, Computational inorganic chemistry—a useful tool, and more, Chemtracts Inorg. Chem. 18 (2005) 595–619.
[12] R. Silaghi-Dumitrescu, I. Silaghi-Dumitrescu, E.D. Coulter, D.M. Kurtz Jr., Computational study of the non-heme iron active site in superoxide reductase and its reaction with superoxide, Inorg. Chem. 42 (2003) 446–456.
[13] A.D. Becke, Density-functional exchange-energy approximation with correct asymptotic behaviour, Phys. Rev. A38 (1988) 3098–3100.
[14] J.P. Perdew, Density-functional approximation for the correlation energy of the inhomogeneous electron gas, Phys. Rev. B33 (1986) 8822–8824.
[15] Spartan 5.0, Wavefunction, Inc., 18401 Von Karman Avenue Suite 370, Irvine, CA, USA.
[16] R. Silaghi-Dumitrescu, The nature of the high-valent complexes in the catalytic cycles of hemoproteins, J. Biol. Inorg. Chem. 9 (2004) 471–476.
[17] R. Silaghi-Dumitrescu, I. Silaghi-Dumitrescu, Hemes revisited by density functional approaches. 1. The axial ligand and the dioxygen-peroxo chemistry, Rev. Roum. Chim. 3–4 (2004) 257–268.
[18] R. Silaghi-Dumitrescu, C.E. Cooper, Transient species involved in catalytic dioxygen/peroxide activation by hemoproteins: possible involvement of protonated Compound I species, Dalton Trans. (2005) 3477–3482.
[19] R. Silaghi-Dumitrescu, I. Silaghi-Dumitrescu, DFT and the electromerism in complexes of iron with diatomic ligands, J. Inorg. Biochem. 100 (2006) 161–166.
[20] R. Silaghi-Dumitrescu, B.J. Reeder, P. Nicholls, C.E. Cooper, M.T. Wilson, Ferryl haem protonation gates peroxidatic reactivity in globins, Biochem. J. 403 (2007) 391–395.
[21] M.T. Kieber-Emmons, J. Annaraj, M.S. Seo, K.M. Van Heuvelen, T. Tosha, T. Kitagawa, T.C. Brunold, W. Nam, C.G. Riordan, Identification of an "end-on" nickel-superoxo adduct, $[Ni(tmc)(O_2)]^+$, J. Am. Chem. Soc. 128 (44) (2006) 14230–14231.
[22] A. Bassan, T. Borowski, P.E. Siegbahn, Quantum chemical studies of dioxygen activation by mononuclear non-heme iron enzymes with the 2-His-1-carboxylate facial triad, Dalton Trans. (2004) 3153–3162.
[23] R. Silaghi-Dumitrescu, Hemes Revisited by Density Functional Approaches. 2. A Paradigm for Axial Ligation in Hemoproteins, 51, Studia Univ. Babes-Bolyai, Chemia, 2006, pp. 167–174.
[24] An essentially identical description was obtained for the S = 0 state, which was ~12 kcal/mol higher in energy than the S = 1 state discussed in text; full geometry optimization of the S = 0 state could not be achieved and the 12 kcal/mol energy is reported for S = 0 at the geometry optimized for S = 1.
[25] D.M. Kurtz Jr., 8.4 dioxygen-binding proteins, in: J.A. McCleverty, T.B. Meyer (Eds.), Comprehensive Coordination Chemistry II—From Biology to Nanotechnology, Elsevier Science, Ltd., 2004.
[26] The water molecule rearranged upon geometry optimization with its oxygen atom away from he nickel, involved in a hydrogen bond with the NH2 protons of the ligand.
[27] A.T. Fiedler, P.A. Bryngelson, M.J. Maroney, T.C. Brunold, Spectroscopic and computational studies of Ni superoxide dismutase: electronic structure contributions to enzymatic function, J. Am. Chem. Soc. 127 (2005) 5449–5462.
[28] A. Yeh, Y. Hu, F.J. Jenney, M. Adams, D. Rees, Structures of the superoxide reductase from *Pyrococcus furiosus* in the oxidized and reduced states, Biochemistry 39 (2000) 2499–2508.
[29] P.E.M. Siegbahn, M.R.A. Blomberg, Density functional theory of biologically relevant metal centers, Annu. Rev. Phys. Chem. 50 (1999) 221–249.
[30] P.E.M. Siegbahn, M.R.A. Blomberg, Metal systems in biochemistry studied by high accuracy quantum chemical methods, Chem. Rev. 100 (2000) 421–437.
[31] G.H. Loew, D.L. Harris, Role of the heme active site and protein environment in structure, spectra, and function of the cytochrome P450s, Chem. Rev. 100 (2000) 407–419.
[32] R. Carrasco, I. Morgenstern-Badarau, J. Cano, Charge transfers influence on the spin ground state of manganese and iron superoxide dismutases: a DFT study of the reduced active site interaction with O_2^{-}, Chem. Commun. (2003) 436–437.
[33] R. Silaghi-Dumitrescu, I. Silaghi-Dumitrescu, E.D. Coulter, J.P. Emerson, D.M. Kurtz Jr., Computational study of the non-heme iron active site in superoxide reductase and its reaction with superoxide, J. Inorg. Biochem. 86 (2001) 432.
[34] R. Silaghi-Dumitrescu, Factors controlling O–O bond cleavage in ferric-hydroperoxo complexes, Proc. Rom. Acad. Ser. B 3 (2004) 155–163.
[35] E.I. Solomon, T.C. Brunold, M.I. Davis, J.N. Kemsley, S.K. Lee, N. Lehnert, N. Neese, A.J. Skulan, Y.S. Yang, Z. Zhou, Geometric and electronic structure/function correlations in non-heme iron enzymes, Chem. Rev. 100 (2000) 235–350.
[36] E.I. Solomon, A. Decker, N. Lehnert, Non-heme iron enzymes: contrasts to heme catalysis, Proc. Natl. Acad. Sci. U.S.A. 100 (2003) 3589–3594.
[37] Y. Watanabe, Alternatives to the oxoferryl porphyrin cation radical as the proposed reactive intermediate of cytochrome P450: two-electron oxidized Fe(III) porphyrin derivatives, J. Biol. Inorg. Chem. 6 (2001) 846–856.
[38] M. Costas, M.P. Mehn, M.P. Jensen, L.J. Que, Dioxygen activation at mononuclear nonheme iron active sites: enzymes, models, and intermediates, Chem. Rev. 2 (2004) 939–986.
[39] A. Wada, S. Ogo, S. Nagatomo, T. Kitagawa, Y. Watanabe, K. Jitsukawa, H. Masuda, Reactivity of hydroperoxide bound to a mononuclear non-heme iron site, Inorg. Chem. 41 (2002) 616–618.
[40] B. Meunier, S.P. de Visser, S. Shaik, Mechanism of oxidation reactions catalyzed by cytochrome p450 enzymes, Chem. Rev. 104 (2004) 3947–3980.
[41] D.M. Kurtz Jr., Microbial detoxification of superoxide: the non-heme iron reductive paradigm for combating oxidative stress, Acc. Chem. Res. 37 (2004) 902–908.
[42] J.A. Kovacs, Synthetic analogues of cysteinate-ligated non-heme iron and non-corrinoid cobalt enzymes, Chem. Rev. 104 (2004) 825–848.
[43] L. Noodleman, T. Lovell, W.G. Han, J. Li, F. Himo, Quantum chemical studies of intermediates and reaction pathways in selected enzymes and catalytic synthetic systems, Chem. Rev. 104 (2004) 459–508.
[44] C.M.T. Mathe, O. Horner, M. Lombard, J.M. Latour, M. Fontecave, V. Niviere, Identification of iron(III) peroxo species in the active site of the superoxide reductase SOR from *Desulfoarculus baarsii*, J. Am. Chem. Soc. 124 (2002) 4966–4967.
[45] C. Mathe, V. Niviere, C. Houee-Levin, T.A. Mattioli, Fe(3+)-eta(2)-peroxo species in superoxide reductase from *Treponema pallidum*. Comparison with *Desulfoarculus baarsii*, Biophys. Chem. 119 (1) (2005) 38–48.
[46] O. Horner, J.M. Mouesca, J.L. Oddou, C. Jeandey, V. Niviere, T.A. Mattioli, C. Mathe, M. Fontecave, P. Maldivi, P. Bonville, J.A. Halfen, J.M. Latour, Mossbauer characterization of an unusual high-spin side-on peroxo-Fe^{3+} species in the active site of superoxide reductase from *Desulfoarculus baarsii*. Density functional calculations on related models, Biochemistry 43 (2004) 8815–8825.
[47] E. Coulter, J. Emerson, D.J. Kurtz, D. Cabelli, Superoxide reactivity of rubredoxin oxidoreductase (desulfoferrodoxin) from *Desulfovibrio vulgaris*: a pulse radiolysis study, J. Am. Chem. Soc. 122 (2000) 11555–11556.
[48] J. Emerson, E. Coulter, D. Cabelli, R. Phillips, D.M.J. Kurtz, Kinetics and mechanism of superoxide reduction by two-iron superoxide reductase from *Desulfovibrio vulgaris*, Biochemistry 41 (2002) 4348–4357.
[49] J.M. Gutteridge, Superoxide dismutase inhibits the superoxide-driven Fenton reaction at two different levels. Implications for a wider protective role, FEBS Lett. 185 (1985) 19–23.
[50] S.D. Copley, Enzymes with extra talents, Curr. Opin. Chem. Biol. 7 (2003) 265–272.
[51] W.L. DeLano, Pymol, The Pymol Molecular Graphics System, Delano Scientific LLC, San Carlos, CA, USA. http://www.pymol.org.